


 Cite this: *RSC Adv.*, 2024, 14, 147

 Received 19th November 2023  
 Accepted 7th December 2023

DOI: 10.1039/d3ra07917a

[rsc.li/rsc-advances](https://rsc.li/rsc-advances)

# Preparation of $\text{ReNiO}_3$ (Re = Pr, Sm, Eu) and proton conductivity

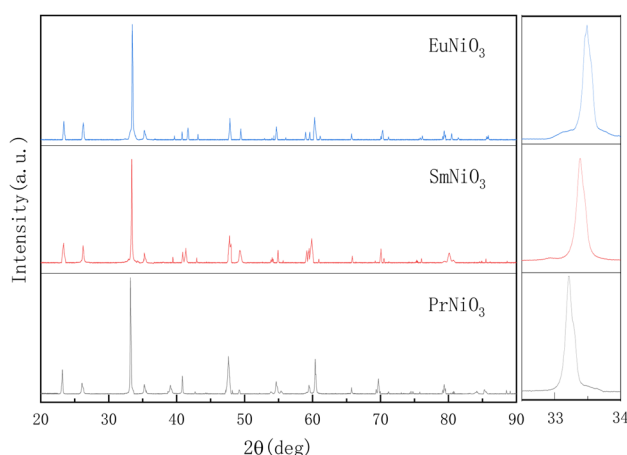
 Hongzheng Li,<sup>ab</sup> Ying Li,<sup>ID</sup> \*<sup>ab</sup> Bo Li,<sup>ab</sup> Wenlong Huang<sup>a</sup> and Yushi Ding<sup>a</sup>

$\text{ReNiO}_3$  (Re = Pr, Sm, Eu) solid electrolytes were prepared by the sol–gel method, which were sintered in a pure oxygen atmosphere of 20 MPa at 1000 °C for 24 hours. The DC resistivities of the three materials in air and in a hydrogen-containing atmosphere were tested respectively. The resistivities in the hydrogen-containing atmosphere were about  $10^2$ ,  $10^4$ , and  $10^5$  times higher than those in air and XPS analysis showed that after 10% $\text{H}_2$ –Ar treatment, the proportion of  $\text{Ni}^{2+}$  of  $\text{PrNiO}_3$ ,  $\text{SmNiO}_3$  and  $\text{EuNiO}_3$  increased successively. The proton transport number of  $\text{PrNiO}_3$  was lower than 0.5 at 50–500 °C, and  $\text{SmNiO}_3$  and  $\text{EuNiO}_3$  were almost pure proton conductors below 200 °C. The conductivities of  $\text{SmNiO}_3$  and  $\text{EuNiO}_3$  were  $1.08 \times 10^{-4} \text{ S cm}^{-1}$  and  $1.83 \times 10^{-5} \text{ S cm}^{-1}$  at 200 °C in 5% $\text{H}_2$ –Ar. The hydrogen sensing properties of  $\text{SmNiO}_3$  and  $\text{EuNiO}_3$  show that the measurement results of the two materials were accurate in the range of 0.5–10%  $\text{H}_2$ .

## 1. Introduction

Proton conductors have always been a focus and research object for fuel cells,<sup>1–3</sup> hydrogen sensors,<sup>4,5</sup> and electrochemical hydrogen separation.<sup>6–8</sup> In any field, researchers want materials with high proton conductivity and proton transport number. It is generally accepted that in order to obtain a higher proton conductivity, a higher proton concentration and a lower proton conduction barrier are required in the material.<sup>9,10</sup> Theoretically, the concentration of oxygen ion vacancies determines the upper limit of proton concentration, so a large dose of dopant is required to produce a high concentration of oxygen ion vacancies, but too high a concentration of dopant may lead to poor stability of the material or the formation of other impurity phases. This indicates that typical perovskite proton conductors such as Y-doped  $\text{BaCeO}_3$  and  $\text{BaZrO}_3$  cannot increase proton concentration without limit by high dose doping. K. D. Kreuer<sup>11</sup> proposed that protons in  $\text{ABO}_3$  perovskite materials with a tetravalent B-site (IV) have a lower transport barrier than in materials with a pentavalent B-site (V). Moreover, the trivalent B-site materials may have higher ionic conductivity. Therefore, some scholars have turned their attention to A(III)–B(III) type materials. Zhou *et al.*<sup>12</sup> first reported that protons can spontaneously bind to  $\text{SmNiO}_3$ , the concentration of protons in  $\text{SmNiO}_3$  may not be limited by the concentration of oxygen vacancies, and high proton conductivity can be obtained in a hydrogen-containing atmosphere at a lower temperature,

which has attracted wide attention.  $\text{SmNiO}_3$  has a perovskite structure; due to its high electronic conductivity,<sup>13,14</sup> it was not paid much attention at first. However, in a hydrogen-containing atmosphere, the material produces a Mott transition due to the inclusion of hydrogen, which inhibits the conduction of electrons,<sup>15,16</sup> which is extremely favorable for enhancing the proton transport of the material. Moreover, the  $\text{BO}_6$  octahedron in  $\text{SmNiO}_3$  is conducive to proton conduction. At present,  $\text{SmNiO}_3$  materials are generally prepared as thin films by vapor deposition or pulsed laser deposition.<sup>12,17,18</sup> In fact, the thin films are affected by the substrate and the thickness of the film,<sup>19,20</sup> and there are deficiencies in the area, uniformity, and repeatability of the films. Therefore, comparison of the different properties of rare earth nickelates would obviously require preparing the material into bulk samples by a conventional sintering method.


 Fig. 1 XRD patterns of  $\text{ReNiO}_3$  (Re = Pr, Sm, Eu).

<sup>a</sup>School of Metallurgy, Northeastern University, China. E-mail: [liying@mail.neu.edu.cn](mailto:liying@mail.neu.edu.cn)
<sup>b</sup>Liaoning Key Laboratory for Metallurgical Sensor Materials and Technology, Northeastern University, China


## 2. Experiment

### 2.1 Preparation of $\text{ReNiO}_3$

To obtain metastable  $\text{Ni}^{3+}$ , high pressure sintering in pure oxygen is required.<sup>13,14,21</sup>  $\text{ReNiO}_3$  (Re = Pr, Sm, Eu) were prepared by the sol-gel method,  $\text{Pr}(\text{NO}_3)_3 \cdot 6\text{H}_2\text{O}$  (99.99%, Aladdin),  $\text{Sm}(\text{NO}_3)_3 \cdot 6\text{H}_2\text{O}$  (99.99%, Aladdin),  $\text{Eu}(\text{NO}_3)_3 \cdot 6\text{H}_2\text{O}$  (99.99%, Aladdin),  $\text{Ni}(\text{NO}_3)_2 \cdot 6\text{H}_2\text{O}$  (99.99%, Aladdin) were accurately weighed according to the ratio and dissolved in water respectively, and the solution temperature was set at 80 °C.

Table 1 Crystal data of  $\text{ReNiO}_3$  (Re = Pr, Sm, Eu)

	<i>a</i> (Å)	<i>b</i> (Å)	<i>c</i> (Å)	Unit cell volume (Å <sup>3</sup> )
PrNiO <sub>3</sub>	5.4132	5.3828	7.6226	222.11
SmNiO <sub>3</sub>	5.4252	5.3373	7.5741	219.32
EuNiO <sub>3</sub>	5.4562	5.2938	7.5359	217.68

EDTA (AR, Aladdin) and citric acid monohydrate (AR, Aladdin) were used as complexing agents, EDTA : citric acid : metal ion = 1 : 1 : 1 (molar ratio). The pH of the solution was adjusted by  $\text{HNO}_3$  and  $\text{NH}_3 \cdot \text{H}_2\text{O}$  to keep it between 6 and 8. As the complexing reaction proceeds, the water evaporates continuously. When the gel was formed, it was transferred to the crucible and heated until the gel was dried to powder. The powder was ground and calcined in pure oxygen at 600 °C for 10 hours to obtain the brown-black precursor powder. The precursor powder was pressed into 10 mm diameter slices by cold isostatic pressure, and then sintered in pure oxygen atmosphere at 20 MPa and 1000 °C for 24 hours (the samples were kept in pure oxygen until cooled to room temperature) to obtain dense ceramic electrolytes.

After XRD (Smart Lab 9 kW) confirmation, the XRD of the three samples is consistent with the patterns of  $\text{ReNiO}_3$  (Re = Pr, Sm, Eu) orthorhombic phases in the database (space group *Pbnm* (No. 62), ICDD reference number 01-079-2453, 01-080-1946, 01-085-2249), indicating that  $\text{ReNiO}_3$  (Re = Pr, Sm, Eu)

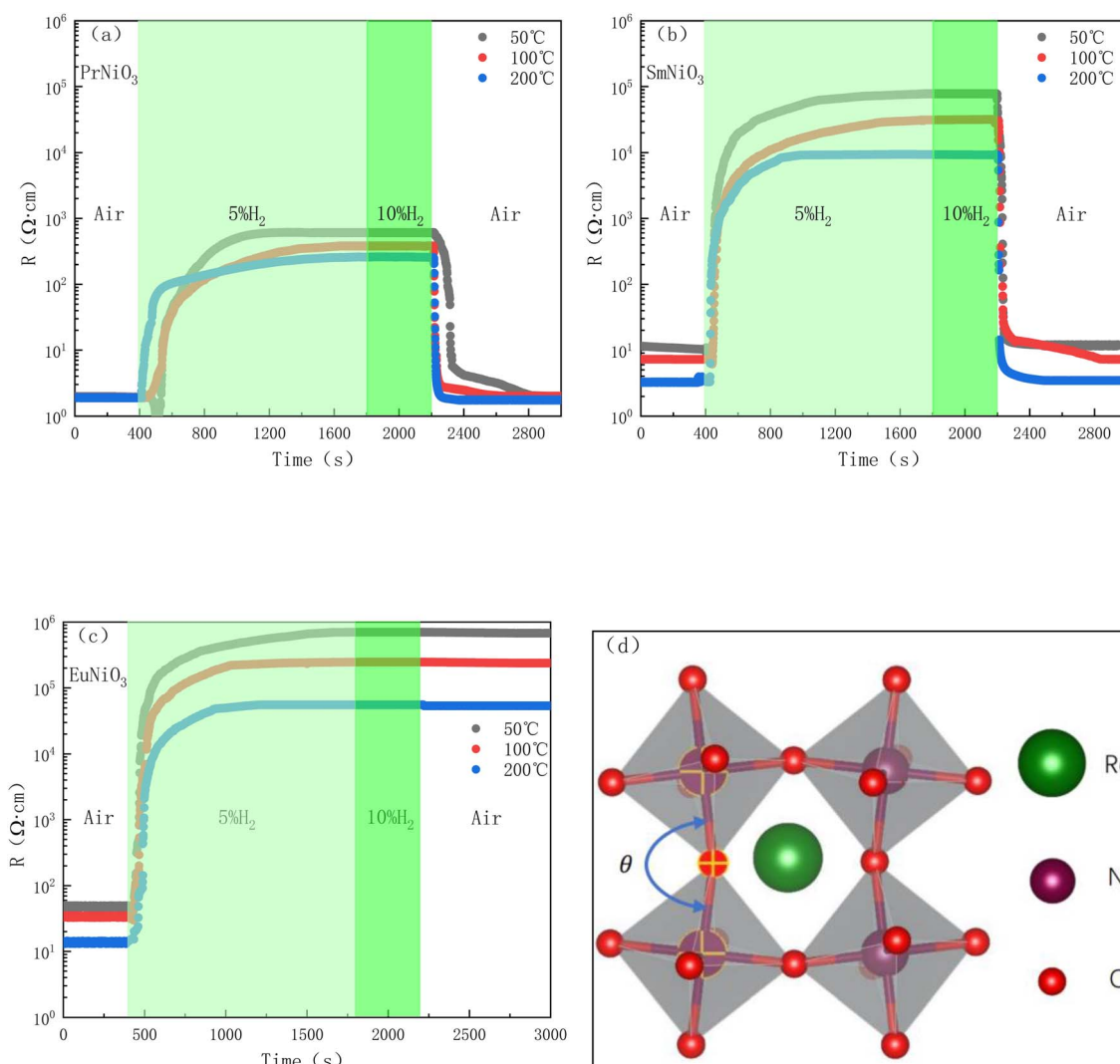


Fig. 2 DC resistivities of three materials in different atmospheres and schematic diagram of crystal structure (a)  $\text{PrNiO}_3$  (b)  $\text{SmNiO}_3$  (c)  $\text{EuNiO}_3$  (d) schematic diagram of  $\text{ReNiO}_3$  crystal structure.



has been successfully synthesized. Fig. 1 shows the XRD patterns of  $\text{ReNiO}_3$  (Re = Pr, Sm, Eu) electrolyte.

Since the ionic radius  $r(\text{Pr}^{3+}) > r(\text{Sm}^{3+}) > r(\text{Eu}^{3+})$ , it can be seen from the local magnification of the main peak that the angle of the diffraction peak gradually shifts to the right. The crystal data after refining are listed in the following table (Table 1):

### 3. Results and discussion

#### 3.1 DC resistivity of $\text{ReNiO}_3$ in different atmospheres

Fig. 2(a–c) show the DC resistivities of  $\text{PrNiO}_3$ ,  $\text{SmNiO}_3$  and  $\text{EuNiO}_3$  in air and hydrogen-containing atmosphere (measured by Keithley 2450, DC voltage is 100 mV, Pt was used as electrode material at two ends of electrolyte).

As shown in Fig. 2, the resistivities of the three materials are low in the air atmosphere for the first 400 s. This is due to the three materials are conductors or semiconductors with very low resistivity in the air,<sup>13,22</sup> and the resistivities increase rapidly after the introduction of 5% $\text{H}_2$ -Ar. After the resistivities reaches

a constant value, the resistivities do not increase even if the concentration of hydrogen increases ( $\sim 1800$  s), and the time to reach equilibrium is shorter as the temperature increases and the resistivities of  $\text{PrNiO}_3$ ,  $\text{SmNiO}_3$  and  $\text{EuNiO}_3$  increases by about  $10^2$ ,  $10^4$  and  $10^5$  times. When air is introduced at 2200 s, the resistivities of  $\text{PrNiO}_3$  and  $\text{SmNiO}_3$  decrease rapidly, and return to the initial resistivities in air around 300–400 s, while the resistivity of  $\text{EuNiO}_3$  is almost unchanged after air introduction (since  $\text{EuNiO}_3$  cannot recover the resistivity, Fig. 2(c) shows the measured curves of three  $\text{EuNiO}_3$  samples of the same size). This is probably due to the reduction of tolerance factor  $t$  as the ion radius of  $\text{Re}^{3+}$  decreases ( $t(\text{PrNiO}_3) = 0.925$ ,  $t(\text{SmNiO}_3) = 0.894$ ,  $t(\text{EuNiO}_3) = 0.887$ ),<sup>21,23</sup> which makes the crystal structure deviate more from the perfect cubic phase ( $t = 1$ ). The bond angle  $\theta$  of Ni–O–Ni becomes smaller (as shown in Fig. 2(d)), and the valence of  $\text{Ni}^{3+}$  becomes more and more unstable<sup>24</sup> and becomes more and more responsive to hydrogen.

Fig. 3 shows the XPS (Thermo Scientific K-Alpha) of the three samples before and after 10% $\text{H}_2$ -Ar treatment. As shown in

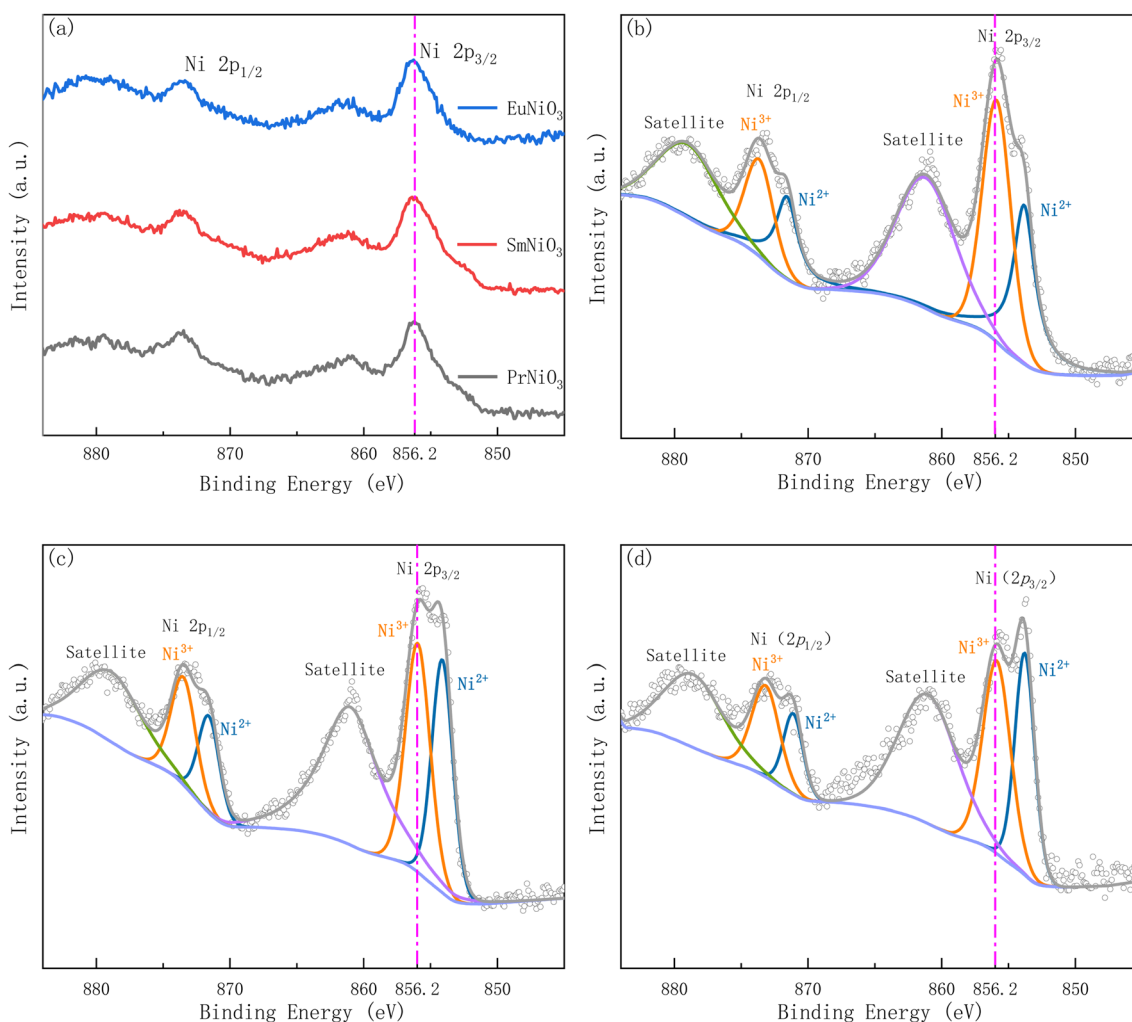


Fig. 3 XPS spectra of three samples before and after 10% $\text{H}_2$ -Ar treatment (a)  $\text{ReNiO}_3$  (Re = Pr, Sm, Eu) before hydrogen treatment (b)  $\text{PrNiO}_3$  after hydrogen treatment (c)  $\text{SmNiO}_3$  after hydrogen treatment (d)  $\text{EuNiO}_3$  after hydrogen treatment.



Fig. 3(a) that the Ni(2p<sub>3/2</sub>) peaks of the three samples before 10%H<sub>2</sub>-Ar treatment are all at the position of 852.2 eV binding energy. The peak at this location is assigned to Ni<sup>3+</sup>.<sup>25,26</sup> However, after 10%H<sub>2</sub>-Ar treatment (the samples were stabilized in 10%H<sub>2</sub>-Ar for 1 hour at 50 °C), the peak of Ni(2p<sub>3/2</sub>) shifted significantly towards the direction of low binding energy, as shown in Fig. 3(b-d), indicating that the average valence state of Ni element decreased. Moreover, after peak-differentiating and imitating of the XPS spectra of the three samples treated with 10%H<sub>2</sub>-Ar, it is found that the peak intensity of the Ni<sup>2+</sup> in PrNiO<sub>3</sub>, SmNiO<sub>3</sub> and EuNiO<sub>3</sub> gradually increases, indicating that the proportion of Ni<sup>2+</sup> is increasing, which is consistent with the trend of increasing resistivity ratio of the three samples in hydrogen and air.

However, this cannot fully explain that EuNiO<sub>3</sub> is irreversible. Some scholars believe that hydrogen insertion will reduce the Gibbs free energy of the system.<sup>27</sup> The smaller ion radius of Re<sup>3+</sup> is, the easier the process of hydrogen insertion will be until EuNiO<sub>3</sub> becomes spontaneous reaction. However, this computing method<sup>28</sup> is the inference which is based on A-site = La, B-site = Fe, Co, Mn elements, and assumes that the oxides in the system are immiscible, which may deviate from the reality.

### 3.2 Measurement of proton transport number

The proton transport number was measured by electromotive force method (Aremco 503 ceramic bond is used as sealant between electrolyte and fixture). According to the formula,

$$E = \frac{RT}{2F} \ln \left( \frac{pH'_2}{pH''_2} \right)$$

$E$  is electromotive force;  $R$  is the ideal gas constant, 8.314 J (mol K)<sup>-1</sup>;  $F$  is Faraday's constant, 96485 C mol<sup>-1</sup>; pH'<sub>2</sub> is 4%H<sub>2</sub>-Ar; pH''<sub>2</sub> is 2%H<sub>2</sub>-Ar.

Therefore, proton transport number( $t_H$ ) is the actual electromotive force ( $E_{act}$ ) ratio of the theoretical electromotive force ( $E_{th}$ ).

Fig. 4(a) shows  $E_{th}$  and  $E_{act}$  of the ReNiO<sub>3</sub>, and Fig. 4(b) shows the proton transport number of the ReNiO<sub>3</sub>.

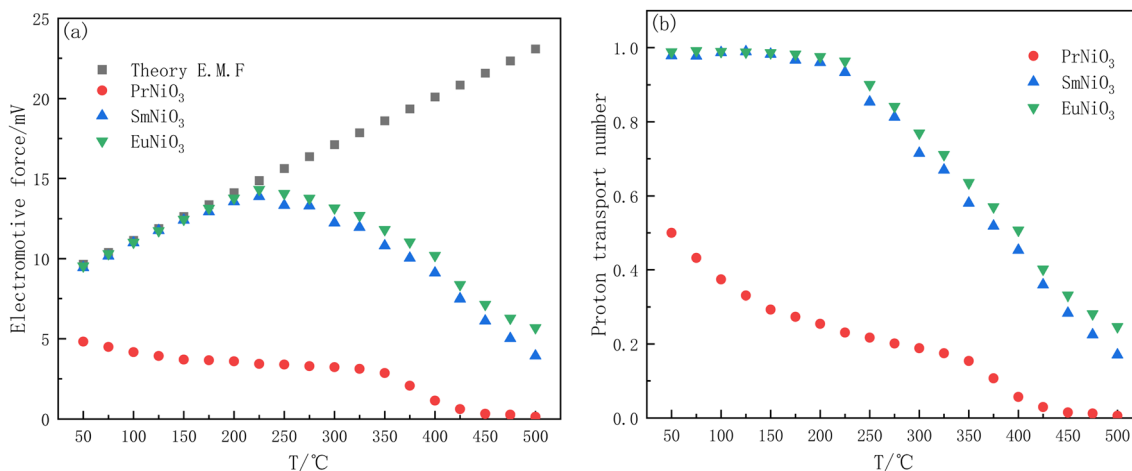


Fig. 4 The EMF (a) and proton transport number (b) of the ReNiO<sub>3</sub>.

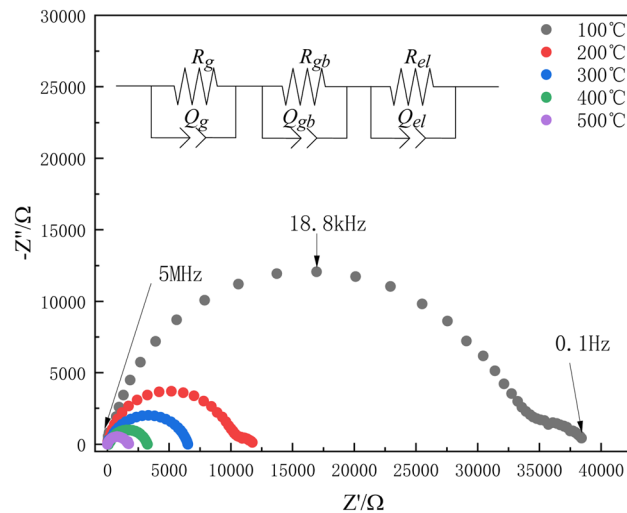


Fig. 5 Partial impedance spectra of SmNiO<sub>3</sub> in 5%H<sub>2</sub>-Ar.

Table 2 The relation between conductivity and temperature of SmNiO<sub>3</sub> and EuNiO<sub>3</sub> (50–200 °C)

Materials	Pre-exponential factor (line intercept)	$E_a$ /eV
SmNiO <sub>3</sub>	2.445	0.220
EuNiO <sub>3</sub>	1.605	0.259

As shown in Fig. 4(b) that the proton transport number of PrNiO<sub>3</sub> is low and always less than 0.5, indicating that proton is not the main carrier in PrNiO<sub>3</sub> and cannot be used as

Table 3 The relation between conductivity and temperature of SmNiO<sub>3</sub> and EuNiO<sub>3</sub> (400–500 °C)

Materials	Pre-exponential factor (line intercept)	$E_a$ /eV
SmNiO <sub>3</sub>	4.398	0.332
EuNiO <sub>3</sub>	4.668	0.417



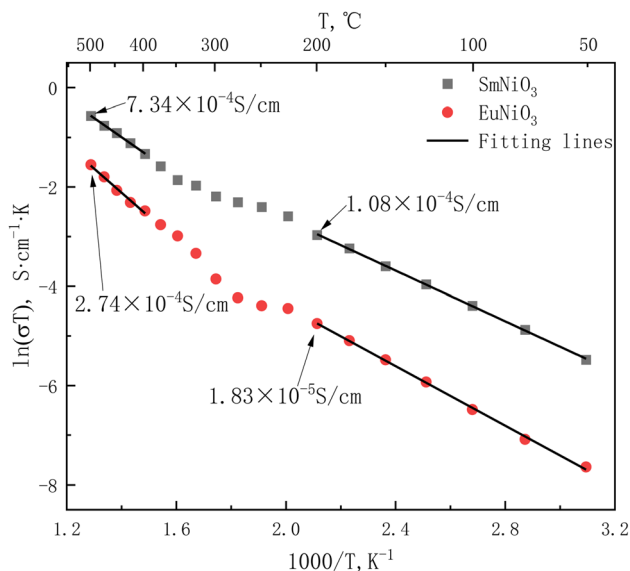


Fig. 6 Arrhenius curves of  $\text{SmNiO}_3$  and  $\text{EuNiO}_3$ .

a proton conductor. When the temperature exceeds  $400\text{ }^\circ\text{C}$ , the actual electromotive force of  $\text{PrNiO}_3$  is almost 0, and the electrolyte is in the state of short circuit. The  $E_{\text{act}}$  of  $\text{SmNiO}_3$

and  $\text{EuNiO}_3$  is very close to the  $E_{\text{th}}$  below  $225\text{ }^\circ\text{C}$ , and the two materials are almost pure proton conductors. The proton transport number decreases with increasing temperature, and the proton transport number of  $\text{EuNiO}_3$  is slightly higher than that of  $\text{SmNiO}_3$ .

### 3.3 Measurement of electrical conductivity

After the  $\text{SmNiO}_3$  and  $\text{EuNiO}_3$  were stabilized in  $5\%\text{H}_2\text{-Ar}$  at  $50\text{ }^\circ\text{C}$  for 30 min, the conductivities of the two samples were measured by AC impedance (Solartron 1260). The frequency range is  $5 \times 10^6\text{-}10^{-1}\text{ Hz}$ , and the AC voltage is 100 mV.

Fig. 5 shows part of the AC impedance spectrum of  $\text{SmNiO}_3$  in  $5\%\text{H}_2\text{-Ar}$ . The circuit in the figure is used for impedance fitting ( $R_b$  represents bulk resistance,  $R_{gb}$  represents grain boundary resistance,  $R_{cl}$  represents resistance of interface or electrode process).

According to AC impedance at different temperatures, the electrical conductivities and activation energy ( $E_a$ ) of the materials were calculated and listed in Tables 2 and 3 and Arrhenius curve are showed in Fig. 6.

Compared with the films prepared by RF magnetron sputtering<sup>12</sup> and pulsed laser deposition,<sup>17</sup> the conductivity of the materials prepared by solid-phase sintering method is about 2 orders of magnitude lower, but the activation energy is slightly

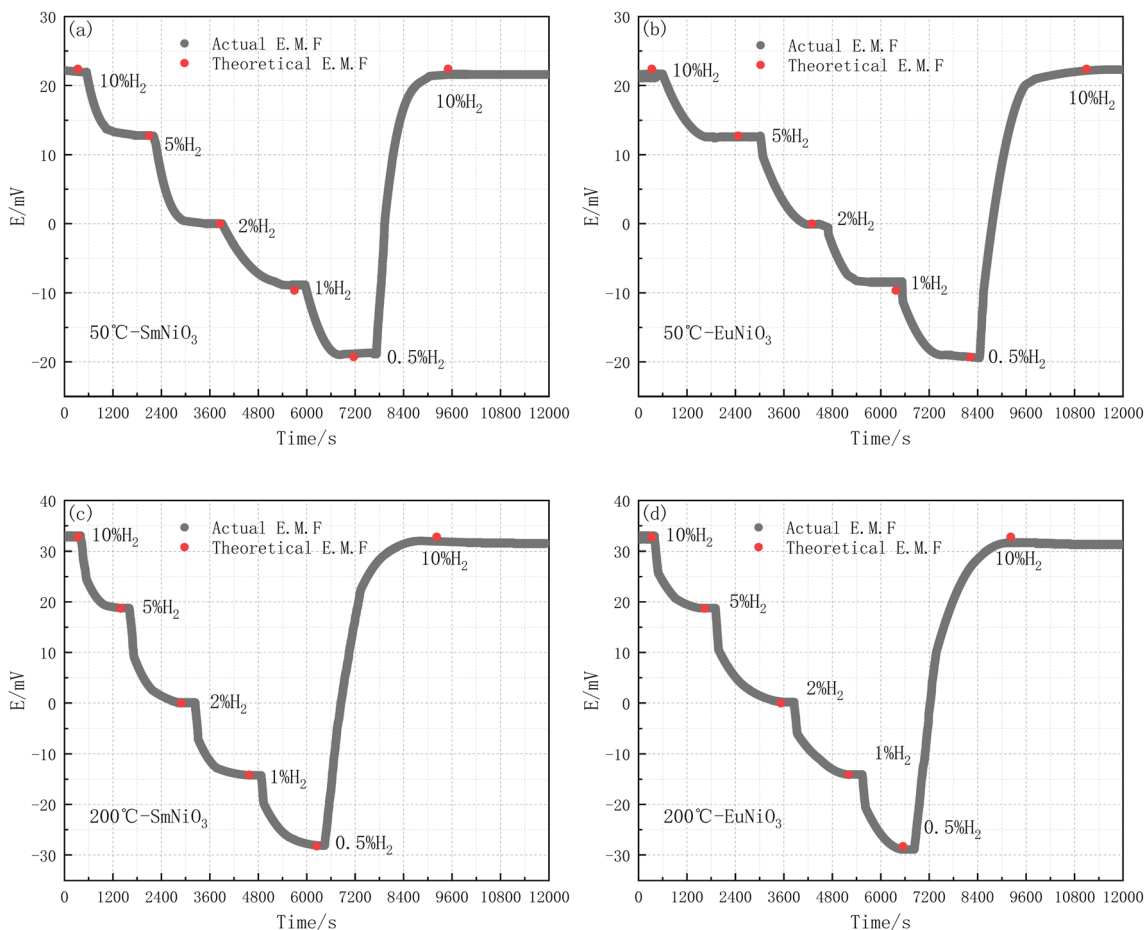


Fig. 7 Hydrogen sensing properties of  $\text{SmNiO}_3$  and  $\text{EuNiO}_3$  (a)  $50\text{ }^\circ\text{C-SmNiO}_3$  (b)  $50\text{ }^\circ\text{C-EuNiO}_3$  (c)  $200\text{ }^\circ\text{C-SmNiO}_3$  (d)  $200\text{ }^\circ\text{C-EuNiO}_3$ .



lower than that of the films (0.23–0.37 eV),<sup>17</sup> indicating that the materials are more likely to transport protons without the influence of substrate.

### 3.4 Hydrogen sensing properties of SmNiO<sub>3</sub> and EuNiO<sub>3</sub>

After the SmNiO<sub>3</sub> and EuNiO<sub>3</sub> electrolyte tablets were stabilized in 2%H<sub>2</sub>-Ar for 30 min, the sensing properties of SmNiO<sub>3</sub> and EuNiO<sub>3</sub> at 50 °C and 200 °C were tested by using 2%H<sub>2</sub>-Ar as a reference gas.

As shown in Fig. 7 that the actual EMF of SmNiO<sub>3</sub> and EuNiO<sub>3</sub> at different hydrogen partial pressures of 50 °C and 200 °C is very close to the theoretical EMF. The time from response to equilibrium for SmNiO<sub>3</sub> and EuNiO<sub>3</sub> at 50 °C is approximately 1800 s, and the time at 200 °C is approximately 1500 s.

## 4. Conclusion

ReNiO<sub>3</sub> (Re = Pr, Sm, Eu) were prepared by the sol-gel method. The sintering conditions were as follows: pure oxygen atmosphere of 20 MPa, sintering at 1000 °C for 24 hours. The DC resistivities of ReNiO<sub>3</sub> (Re = Pr, Sm, Eu) in a hydrogen-containing atmosphere are about 10<sup>2</sup>, 10<sup>4</sup>, and 10<sup>5</sup> times higher than in air. XPS analysis shows that after hydrogen treatment, the proportion of Ni<sup>2+</sup> in PrNiO<sub>3</sub>, SmNiO<sub>3</sub> and EuNiO<sub>3</sub> increased successively, which was consistent with the trend of increasing resistivity ratio. The electromotive force method was used to measure the proton transport number of the three materials. The results show that the proton transport number ( $t_{\text{H}}$ ) of PrNiO<sub>3</sub> is always lower than 0.5 in the test temperature range, and almost 0 when the temperature is higher than 400 °C. SmNiO<sub>3</sub> and EuNiO<sub>3</sub> are almost pure proton conductors below 200 °C, and the proton transport number decreases gradually with the increasing temperature. The conductivities of SmNiO<sub>3</sub> and EuNiO<sub>3</sub> are measured by AC impedance in 5%H<sub>2</sub>-Ar. The results show that the conductivities of SmNiO<sub>3</sub> and EuNiO<sub>3</sub> are  $1.08 \times 10^{-4}$  S cm<sup>-1</sup> and  $1.83 \times 10^{-5}$  S cm<sup>-1</sup> at 200 °C. The conductivities are  $7.34 \times 10^{-4}$  S cm<sup>-1</sup> and  $2.74 \times 10^{-4}$  S cm<sup>-1</sup> at 500 °C. The activation energies ( $E_{\text{a}}$ ) of SmNiO<sub>3</sub> are 0.220 eV (50–200 °C) and 0.332 eV (400–500 °C), and those of EuNiO<sub>3</sub> are 0.259 eV (50–200 °C) and 0.417 eV (400–500 °C). The hydrogen sensing properties of SmNiO<sub>3</sub> and EuNiO<sub>3</sub> show that the measurement results of both materials are accurate in the range of 0.5–10%H<sub>2</sub>. The equilibrium time is about 1800 s at 50 °C and 1500 s at 200 °C.

## Conflicts of interest

There are no conflicts to declare.

## Acknowledgements

This work was financially supported by the National Natural Science Foundation of China (Project No. 51834004 and 51774076) and the Fundamental Research Funds for the Central Universities (Project No. N2225018).

## References

- 1 K. D. Kreuer, Proton-Conducting Oxides, *Annu. Rev. Mater. Res.*, 2003, **33**, 333–359, DOI: [10.1146/annurev.matsci.33.022802.091825](https://doi.org/10.1146/annurev.matsci.33.022802.091825).
- 2 D. Pergolesi, E. Fabbri, A. D'Epifanio, E. Di Bartolomeo, A. Tebano, S. Sanna, S. Licocchia, G. Balestrino and E. Traversa, High proton conduction in grain-boundary-free yttrium-doped barium zirconate films grown by pulsed laser deposition, *Nat. Mater.*, 2010, **9**, 846–852, DOI: [10.1038/nmat2837](https://doi.org/10.1038/nmat2837).
- 3 F. S. da Silva and T. M. de Souza, Novel materials for solid oxide fuel cell technologies: A literature review, *Int. J. Hydrogen Energy*, 2017, **42**, 26020–26036, DOI: [10.1016/j.ijhydene.2017.08.105](https://doi.org/10.1016/j.ijhydene.2017.08.105).
- 4 P. Pasierb, A. Biernacka-Such, S. Komornicki and M. Rekas, Application of proton-conducting SrCeO<sub>3</sub> for construction of potentiometric hydrogen gas sensor, *Proc. SPIE*, 2006, **6348**, 634806, DOI: [10.1117/12.721037](https://doi.org/10.1117/12.721037).
- 5 A. Kalyakin, A. Volkov, J. Lyagaeva, D. Medvedev, A. Demin and P. Tsiakaras, Combined amperometric and potentiometric hydrogen sensors based on BaCe<sub>0.7</sub>Zr<sub>0.1</sub>Y<sub>0.2</sub>O<sub>3-δ</sub> proton-conducting ceramic, *Sens. Actuators, B*, 2016, **231**, 175–182, DOI: [10.1016/j.snb.2016.03.017](https://doi.org/10.1016/j.snb.2016.03.017).
- 6 J. W. Phair and S. P. S. Badwal, Review of proton conductors for hydrogen separation, *Ionics*, 2006, **12**, 103–115, DOI: [10.1007/s11581-006-0016-4](https://doi.org/10.1007/s11581-006-0016-4).
- 7 H. Matsumoto, T. Shimura, H. Iwahara, T. Higuchi, K. Yashiro, A. Kaimai, T. Kawada and J. Mizusaki, Hydrogen separation using proton-conducting perovskites, *J. Alloys Compd.*, 2006, **408–412**, 456–462, DOI: [10.1016/j.jallcom.2004.12.093](https://doi.org/10.1016/j.jallcom.2004.12.093).
- 8 S. Robinson, A. Manerbino and W. Grover Coors, Galvanic hydrogen pumping in the protonic ceramic perovskite BaCe<sub>0.2</sub>Zr<sub>0.7</sub>Y<sub>0.1</sub>O<sub>3-δ</sub>, *J. Membr. Sci.*, 2013, **446**, 99–105, DOI: [10.1016/j.memsci.2013.06.026](https://doi.org/10.1016/j.memsci.2013.06.026).
- 9 M. Cherry, M. S. Islam, J. D. Gale and C. R. A. Catlow, Computational studies of protons in perovskite-structured oxides, *J. Phys. Chem.*, 1995, **99**, 14614–14618, DOI: [10.1021/j100040a007](https://doi.org/10.1021/j100040a007).
- 10 M. S. Islam, S. Wang, A. M. Nolan and Y. Mo, First-Principles Computational Design and Discovery of Novel Double-Perovskite Proton Conductors, *Chem. Mater.*, 2021, **33**, 8278–8288, DOI: [10.1021/acs.chemmater.1c02432](https://doi.org/10.1021/acs.chemmater.1c02432).
- 11 K. D. Kreuer, On the complexity of proton conduction phenomena, *Solid State Ion.*, 2000, **136–137**, 149–160, DOI: [10.1016/S0167-2738\(00\)00301-5](https://doi.org/10.1016/S0167-2738(00)00301-5).
- 12 Y. Zhou, X. Guan, H. Zhou, K. Ramadoss, S. Adam, H. Liu, S. Lee, J. Shi, M. Tsuchiya, D. D. Fong and S. Ramanathan, Strongly correlated perovskite fuel cells, *Nature*, 2016, **534**, 231–234, DOI: [10.1038/nature17653](https://doi.org/10.1038/nature17653).
- 13 P. Lacorre, J. Pannetier, S. A. I. Nazzal, P. W. Wang, T. C. Huang, P. Lacorre, J. B. Torrance, J. Pannetier, S. A. I. Nazzal and P. W. Wang, *J. Solid State Chem.*, 1991, **237**, 225–237.



- 14 J. Pérez-Cacho, J. Blasco, J. García, M. Castro and J. Stankiewicz, Study of the phase transitions in SmNiO<sub>3</sub>, *J. Phys.: Condens. Matter*, 1999, **11**, 405–415, DOI: [10.1088/0953-8984/11/2/007](https://doi.org/10.1088/0953-8984/11/2/007).
- 15 P. Yoo and P. Liao, Metal-to-insulator transition in SmNiO<sub>3</sub> induced by chemical doping: A first principles study, *Mol. Syst. Des. Eng.*, 2018, **3**, 264–274, DOI: [10.1039/c8me00002f](https://doi.org/10.1039/c8me00002f).
- 16 J. Shi, Y. Zhou and S. Ramanathan, Colossal resistance switching and band gap modulation in a perovskite nickelate by electron doping, *Nat. Commun.*, 2014, **5**, 4860, DOI: [10.1038/ncomms5860](https://doi.org/10.1038/ncomms5860).
- 17 X. Xu, C. Liu, J. Ma, A. J. Jacobson, C. Nan and C. Chen, Physicochemical properties of proton-conducting SmNiO<sub>3</sub> epitaxial films, *J. Mater.*, 2019, **5**, 247–251, DOI: [10.1016/j.jmat.2019.01.011](https://doi.org/10.1016/j.jmat.2019.01.011).
- 18 Z. Zhang, D. Schwanz, B. Narayanan, M. Kotiuga, J. A. Dura, M. Cherukara, H. Zhou, J. W. Freeland, J. Li, R. Sutarto, F. He, C. Wu, J. Zhu, Y. Sun, K. Ramadoss, S. S. Nonnenmann, N. Yu, R. Comin, K. M. Rabe, S. K. R. S. Sankaranarayanan and S. Ramanathan, Perovskite nickelates as electric-field sensors in salt water, *Nature*, 2018, **553**, 68–72, DOI: [10.1038/nature25008](https://doi.org/10.1038/nature25008).
- 19 T. Higuchi, T. Owaku, Y. Iida, E. Sakai, M. Kobayashi and H. Kumigashira, Proton conduction of BaCe<sub>0.90</sub>Y<sub>0.10</sub>O<sub>3-δ</sub> Thin film with lattice distortion, *Solid State Ion.*, 2015, **270**, 1–5, DOI: [10.1016/j.ssi.2014.11.016](https://doi.org/10.1016/j.ssi.2014.11.016).
- 20 N. Sata, H. Matsuta, Y. Akiyama, Y. Chiba, S. Shin and M. Ishigame, Fabrication of proton conducting thin films of SrZrO<sub>3</sub> and SrCeO<sub>3</sub> and their fundamental characterization, *Solid State Ion.*, 1997, **97**, 437–441, DOI: [10.1016/S0167-2738\(97\)00026-X](https://doi.org/10.1016/S0167-2738(97)00026-X).
- 21 H. Falcón, M. J. Martínez-Lope, J. A. Alonso and J. L. G. Fierro, Large enhancement of the catalytic activity for CO oxidation on hole doped (Ln,Sr)NiO<sub>3</sub> (Ln = Pr, Sm, Eu) Perovskites, *Solid State Ion.*, 2000, **131**, 237–248, DOI: [10.1016/S0167-2738\(00\)00664-0](https://doi.org/10.1016/S0167-2738(00)00664-0).
- 22 R. Lengsdorf, A. Barla, J. A. Alonso, M. J. Martínez-Lope, H. Micklitz and M. M. Abd-Elmeguid, The observation of the insulator-metal transition in EuNiO<sub>3</sub> under high pressure, *J. Phys.: Condens. Matter*, 2004, **16**, 3355–3360, DOI: [10.1088/0953-8984/16/20/006](https://doi.org/10.1088/0953-8984/16/20/006).
- 23 J. A. Alonso, M. J. Martínez-Lope, M. T. Casais, M. A. G. Aranda and M. T. Fernández-Díaz, Metal-insulator transitions, structural and microstructural evolution of RNiO<sub>3</sub> (R = Sm, Eu, Gd, Dy, Ho, Y) perovskites: Evidence for room-temperature charge disproportionation in monoclinic HoNiO<sub>3</sub> and YNiO<sub>3</sub>, *J. Am. Chem. Soc.*, 1999, **121**, 4754–4762, DOI: [10.1021/ja984015x](https://doi.org/10.1021/ja984015x).
- 24 J. B. Torrance, P. Lacorre, A. I. Nazzari, E. J. Ansaldo and C. Niedermayer, Systematic study of insulator-metal transitions in perovskites RNiO<sub>3</sub> (R=Pr,Nd,Sm,Eu) due to closing of charge-transfer gap, *Phys. Rev. B: Condens. Matter Mater. Phys.*, 1992, **45**, 8209–8212, DOI: [10.1103/PhysRevB.45.8209](https://doi.org/10.1103/PhysRevB.45.8209).
- 25 M. W. Roberts and R. S. C. Smart, The defect structure of nickel oxide surfaces as revealed by photoelectron spectroscopy, *J. Chem. Soc., Faraday Trans. 1*, 1984, **80**, 2957–2968, DOI: [10.1039/F19848002957](https://doi.org/10.1039/F19848002957).
- 26 A. F. Carley, S. D. Jackson, J. N. O'Shea and M. W. Roberts, The formation and characterisation of Ni<sup>3+</sup>—an X-ray photoelectron spectroscopic investigation of potassium-doped Ni(110)-O, *Surf. Sci.*, 1999, **440**, L868–L874, DOI: [10.1016/S0039-6028\(99\)00872-9](https://doi.org/10.1016/S0039-6028(99)00872-9).
- 27 J. Chen, Y. Zhou, S. Middey, J. Jiang, N. Chen, L. Chen, X. Shi, M. Döbeli, J. Shi, J. Chakhalian and S. Ramanathan, Self-limited kinetics of electron doping in correlated oxides, *Appl. Phys. Lett.*, 2015, **107**(3), 031905, DOI: [10.1063/1.4927322](https://doi.org/10.1063/1.4927322).
- 28 R. Jaramillo, F. Schoofs, S. D. Ha and S. Ramanathan, High pressure synthesis of SmNiO<sub>3</sub> thin films and implications for thermodynamics of the nickelates, *J. Mater. Chem. C*, 2013, **1**, 2455–2462, DOI: [10.1039/c3tc00844d](https://doi.org/10.1039/c3tc00844d).

